LIQUID CRYSTALS, 2000, VOL. 27, NO. 4, 509–521

Columnar phases of achiral vanadyl liquid crystalline complexes

D. KILIAN†, D. KNAWBY‡, M. A. ATHANASSOPOULOU†,
S. T. TRZASKA‡, T. M. SWAGER‡, S. WRÓBEL§† and W. HAASE†*

†Institut für Physikalische Chemie, Technische Universität Darmstadt,
Petersenstr. 20, D-64287 Darmstadt, Germany
‡Department of Chemistry, Massachusetts Institute of Technology, Cambridge,
MA 02139-4307, USA
§Jagiellonian University, M. Smoluchowski Institute of Physics, 30-059 Kraków,
Reymonta 4, Poland

(*Received 7 June 1999; in final form 28 October 1999; accepted 1 November 1999*)

Two liquid crystalline vanadyl complexes have been studied by frequency domain dielectric spectroscopy over the range 10 mHz to 13 MHz. The materials exhibit two or three columnar phases denoted Col_{ro}, Col_{rd}, and Col_{hd} that were identified by X-ray diffraction. In the higher temperature Col_{rd} phase, a relaxation process in the kHz range is observed that is attributed to the reorientation about the molecular short axis. A pronounced dielectric relaxation process shows up in the low temperature Col_{ro} phase at hertz and sub-hertz frequencies. This slow relaxation is assigned to reorientation of the molecular dipoles within the polar linear chains, which are aligned along the column's axis. Triangular wave switching studies at low frequency reveal processes inside the Col_{ro} phase which are most probably due to ionic/charges relaxations but a ferroelectric switching for an achiral discotic system cannot be ruled out completely. Below the Col_{ro} phase there is an orientationally disordered crystalline Cr_x phase with disordered side chain dipoles. A dielectric relaxation process connected with the intramolecular relaxation of the alkoxy side chains, similar to the β-process of polymers, has been found in the lower temperature Cr_x phase.

1. Introduction

Since the discovery of ferroelectric [1] and antiferroelectric liquid crystals [2] there has been great interest in designing liquid crystals with such properties. Novel schemes have recently resulted in the introduction of ferroelectric properties in systems composed of non-chiral materials based upon low molar mass banana-shaped molecules [3] and exhibiting different smectic-like ordering with in-plane spontaneous polarization. The first example of a ferroelectric liquid crystal based on achiral molecules was demonstrated by Tournilhac *et al.* [4]. It is worth noting that a related achiral mesogenic polymer-monomer mixture [5, 6] also displayed a pronounced spontaneous polarization.

Dielectric spectroscopy was shown by Athanassopoulou *et al.* [7] to be a powerful method for investigation of the dynamics of metallomesogenic ferroelectric materials based on vanadyl, copper and palladium chiral complexes [8, 9]. Indeed, in addition to the rotational and reorientation relaxation, these measurements have revealed collective Goldstone mode processes that are the result of chirality-based symmetry breaking [8, 9].

In this paper we report on further properties of two vanadyl complexes [10–12] which display columnar mesophases with anomalous dielectric behaviour at frequencies below 10 kHz, where a pronounced dielectric spectrum was found. Also for a liquid crystalline mixture containing copper mesogens [7], an anomalous dielectric behaviour was observed earlier and also for some mixtures of two metallomesogenes [13].

In pursuit of novel liquid crystalline metallomesogens, Swager and co-workers [10–12, 14–18] have developed liquid crystalline materials containing polar metal-oxo linear chain polymers, schematically $(\ldots M{=}O\ldots M{=}O\ldots)_n$, as shown in figure 1. Columnar mesophases of these materials show very interesting macroscopic properties and the substances studied in this work exhibit strong

*Author for correspondence;
e-mail: Jochem@hrz2.tu-darmstadt.de

Liquid Crystals ISSN 0267-8292 print/ISSN 1366-5855 online © 2000 Taylor & Francis Ltd
http://www.tandf.co.uk/journals/tf/02678292.html

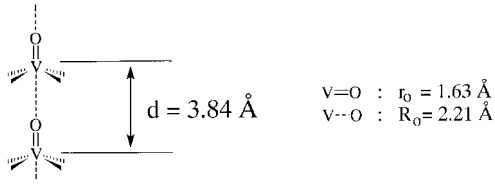

Figure 1. General structure of vanadyl linear chain complexes. Bond lengths are from a related crystal structure [10].

linear chains along the columnar axis, which are characterized by low energy V=O stretching modes at 854 to 868 cm^{-1} depending on the phase. The polar oligomers disassemble in the isotropic phase and a V=O stretching mode of 992 to 994 cm^{-1} [12] characteristic of monomeric complexes is observed.

It should be stressed, that the vanadyl complexes studied in this work (figure 2) do not exhibit an ideal disc-like shape, which is a general feature of thermotropic columnar liquid crystalline phases. According to Swager's model [12] the columnar phases of these substances have short range intermolecular correlation along the column wherein neighbour pairs assemble in an arrangement such as to produce disc-like entities.

It is also interesting that the linear chain derivatives **1**(*n*) (figure 2) display a number of columnar mesophases that have either ordered rectangular lattices (Col_{ro}) or liquid-like disordered structures (Col_{rd} or Col_{hd}). Liquid-like columnar phases display XRD patterns with diffuse halos at wide angles, whereas the ordered phases display more defined wide angle peaks. This study presents additional XRD results, *vide infra*, which require some revisions of the earlier assignments [12]. For the two vanadyl complexes studied, the low temperature phase is characterized as a Col_{ro} phase, whereas the sequentially higher temperature phases are Col_{rd} or Col_{hd} phases, respectively.

The principal aim of this paper is to study the properties of these liquid crystals by low frequency dielectric relaxation spectroscopy. Moreover we seek to establish that this behaviour is the result of long range order of the one dimensional polar linear chains (figure 1) in the Col_{ro} columnar phase and that this effect is lost in the higher temperature phases with only short range order.

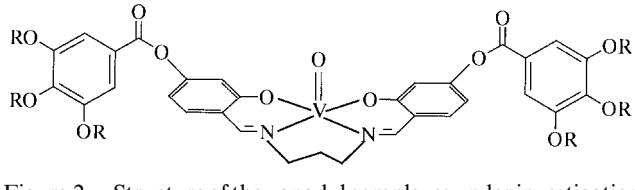

Figure 2. Structure of the vanadyl complexes under investigation with *R* equal to $C_{12}H_{25}$ = **1**(12) and $C_{14}H_{29}$ = **1**(14).

To make the critical structure/property correlation, we have performed a detailed characterization of these novel liquid crystals by DSC, polarizing optical microscopy, XRD, dielectric spectroscopy, and polarization switching.

2. Theoretical background

The application of a weak low frequency electric field, $\mathbf{E}_0 \exp(i\omega t)$, to a dielectric material induces a net polarization:

$$\mathbf{P} = \epsilon_0[\varepsilon^*(\omega) - 1]\,\mathbf{E}_0 \exp(i\omega t) \tag{1}$$

where $\varepsilon^*(\omega)$ is a complex dielectric permittivity and ϵ_0 is the dielectric permittivity of the free space. The static dielectric permittivity, ε_0 ($\varepsilon_0 = \varepsilon^*(0)$) may contain contributions from different molecular and collective relaxation processes. Generally, one can write:

$$\varepsilon_0 = \varepsilon_\infty + \sum_{i,1}^{m} \Delta\varepsilon_i \tag{2}$$

where ε_∞ is the high frequency limit of the dielectric permittivity and $\Delta\varepsilon_i$ is the dielectric contribution from different molecular and collective processes such as molecular reorientation, collective columnar relaxation, space charge relaxation and intramolecular relaxation of side chains.

In the case of columnar phases of complexes displaying a strong vanadyl linear chain structure [12], we are principally concerned with contributions from reorientation of the large dipoles associated with the V=O bond. If switching can occur then it is most probably by an inversion about the vanadyl centre. If each column bears an effective polarization, $\mathbf{P}_{ci}$, the low frequency electric field, due to linear coupling with polarization vectors, induces a pronounced linear polarization comparable to the Goldstone mode contribution in the case of helicoidal FLCs [19].

If true spontaneous polarization $\mathbf{P}_s$ exists then it is connected with the columnar polar chains due to the . . . V=O---V. . . coupling shown in figure 1 and could be written as:

$$\mathbf{P}_s = V^{-1} \sum_{j=1}^{k} \mu_j \tag{3}$$

where μ_j is a dipole moment of the O. . . [. . . V=O. . .]. . . fragment in the columnar chain, V is the unit cell volume, and k stands for the number of dipole moments in the unit cell—$k = 2$ for the Col_{ro} phase.

The dielectric permittivity of the system composed of polarized columns can be described by the Kirkwood formula [20] (4) applied to highly polar liquids. This equation provides the temperature dependence of the static dielectric permittivity of a liquid and is an

extension of the Onsager formula [21].

$$\frac{(\varepsilon_0 - \varepsilon_\infty)(2\varepsilon_0 + \varepsilon_\infty)}{\varepsilon_0(\varepsilon_\infty + 2)^2} = \frac{4\pi N_0}{9k_B T}\mu^2 g \tag{4}$$

where ε_∞ is the high frequency limit of the dielectric permittivity, N_0 is the number of molecules per unit volume, μ is a molecular dipole moment, k_B is Boltzmann's constant, and g is the so-called Kirkwood factor connected with some intermolecular correlation. This Kirkwood factor g is defined in the following way [21]:

$$g = 1 + \frac{1}{Z}\sum_{j \neq i}^{z} \cos \gamma_{ij} \tag{5}$$

where in turn Z is the coordination number (i.e. the number of nearest neighbours of the i-th molecule), and γ_{ij} is the angle between the dipole moment of the i-th molecule and the dipole moment of its j-th neighbour in the first coordination sphere. The Onsager model corresponds to $g = 1$. A value of $g > 1$ indicates an enhanced dipole–dipole correlation of a given molecule with its surroundings, which typically originates from molecular interactions such as hydrogen bonds or steric effects. Alternatively, a reduced dipole–dipole correlation can produce $g < 1$ and this results from steric effects and/or antiparallel dipole–dipole interactions. A value of $g = 0$ indicates that $\varepsilon_0 = \varepsilon_\infty$ which represents an ideal antiparallel organization of the dipoles in the lattice. It is worth pointing out that for ordered dipolar chains, a correlation factor $g = 2$ is expected, assuming parallel nearest neighbour interactions.

In the case of the two solid phases, as well as the columnar rectangular and hexagonal phases, one can use a model by Fröhlich [20, 21]:

$$\frac{(\varepsilon_0 - \varepsilon_\infty)(2\varepsilon_0 + n^2)}{\varepsilon_0} = \frac{4\pi N_0}{9k_B T}\mu^2 g 4w(1 - w) \tag{6}$$

where n is the refractive index, and w is a probability of finding a dipole in a certain direction, given by:

$$w = \frac{\exp[-U(T)/k_B T]}{1 + \exp[-U(T)/k_B T]} \tag{7}$$

where $U(T)$ is a potential barrier hindering reorientation of dipoles. The Fröhlich model is a one-dimensional model, but it is the only model known in the literature to describe the $\varepsilon_0(T)$ temperature behaviour in the vincinity of a molecular order–disorder transition.

To describe the dielectric spectrum of the columnar mesophases, one should take into account the relaxation of the polar columns and the reorientation of individual molecules and molecular segments. In the low frequency range there are ubiquitous contributions from space-charge relaxation and conductivity. Consideration of all four types of relaxation processes provides the following dielectric spectrum:

$$\varepsilon^*(\omega) = \varepsilon' - i\varepsilon'' = \varepsilon_\infty + \frac{\Delta\varepsilon_M}{1 + (i\omega\tau_M)^{1-\alpha M}} + \frac{\Delta\varepsilon_C}{1 + (i\omega\tau_C)^{1-\alpha C}} + \frac{\Delta\varepsilon_0}{1 + (i\omega\tau_0)^{1-\alpha 0}} - i\frac{\sigma}{\in_0 \omega} \tag{8}$$

where σ is the electrical conductivity of the material studied and τ_M, τ_C and τ_0 are, respectively, the average molecular reorientation, columnar and space charge relaxation times. The parameters α_M, α_C and α_0 account for the distribution of the respective relaxation times. In the columnar phase there will be two absorption peaks at frequencies of $1/2\,\tau_M$ and $1/2\,\tau_C$. The space-charge relaxation is activated in the higher temperature phases and in the isotropic phase. It is important to note that in the case of metallomesogens, unavoidable ionic impurities cause the low frequency components of the dielectric spectrum to be dominated by the conductivity (σ/ω) term. It is also the case that the low frequency dielectric relaxation can be easily observed in the loss factor of the dielectric spectrum:

$$\tan \delta(\omega) = \varepsilon''(\omega)/\varepsilon'(\omega) \tag{9}$$

which may be directly measured with an impedance analyser. Additionally, for highly polar dielectrics, the absorption peak of $\tan \delta(\omega)$ is at higher frequencies than that of $\varepsilon''(\omega)$. Hence, the following transformation is valid:

$$\omega_c(\tan \delta) = \omega_c(\varepsilon'')\left(\frac{\varepsilon_0}{\varepsilon_\infty}\right)^{1/2}. \tag{10}$$

It follows for highly polar systems that the absorption peaks of dielectric loss will be shifted to distinctly lower frequencies than observed in the $\tan \delta(\omega)$ dielectric spectrum. This situation is observed for all of substances investigated herein.

3. Experimental

The substances studied have the chemical formula displayed in figure 2. The studies of phase transitions were performed utilizing a DSC (Perkin Elmer DSC 2 with home-made interface for data acquisition), a Leitz Orthoplan Pol polarizing microscope, equipped with video (SONY video cameras, video mixer, video printer, video tape recorder and monitor), and a Mettler hot stage FP82 with controller. The DSC calorimetry was performed at a heating rate of 10 K min^{-1}. In general, a baseline was calibrated before the measurements and was then subtracted from all graphs. It is evident that the mesophase to isotropic transition and the transitions

to columnar mesophases are first order. Therefore the temperatures of these transitions were evaluated by the *T*-onset method [22]. All other phase transition temperatures are reported as the peak maxima of the heat flow vs. temperature profile.

The phase transition temperatures (table 1) were determined by DSC calorimetry, and the first runs are displayed in figure 3. The phases were assigned as: two crystalline (Cr_1, Cr_2), one orientationally disordered crystalline (Cr_x), three discotic columnar mesophases (Col_{ro}, Col_{rd}, Col_{hd}) and the isotropic phase (I).

The conclusion from the DSC, polarizing microscopy, and dielectric spectroscopy is that both samples exhibit at least two discotic columnar liquid crystalline phases. The colour photographs in figure 4 show typical textures observed for different phases, and recorded by the video system.

Table 1. Phase sequence and phase transition temperatures for complexes **1**(12) and **1**(14).

Complex	Transition temperatures obtained by DSC
1(12)	Cr_1 48.5°C Cr_2 68°C Cr_x 97.1°C Col_{ro} 140.9°C Col_{rd} 157.6°C Col_{hd} 182.2°C I
1(14)	Cr_1 68°C Cr_2 82°C Cr_x 89.6°C Col_{ro} 134.9°C Col_{hd} 187.9°C I

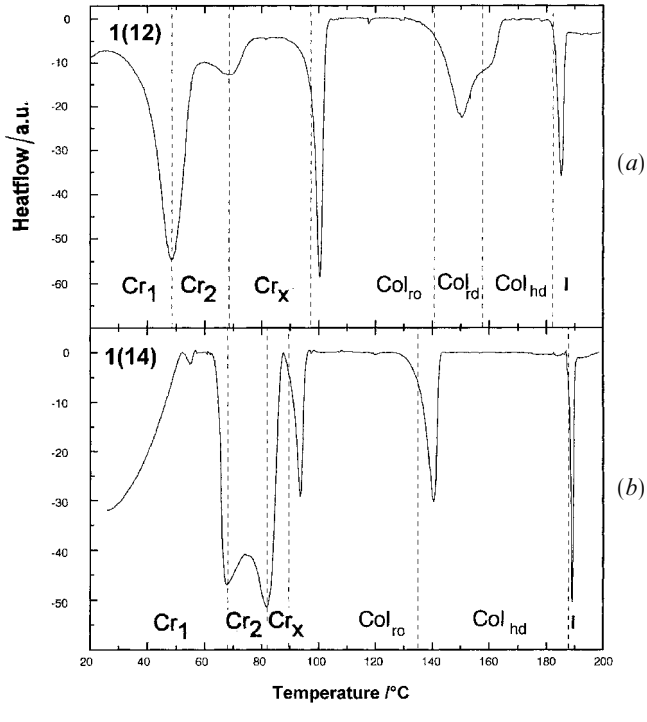

Figure 3. DSC data obtained on heating for (*a*) complex **1**(12) and for (*b*) complex **1**(14).

The X-ray diffraction measurements were performed on a focusing horizontal two-circle diffractometer [23, 24] (Stoe Stadi 2) equipped with a home made oven. The CuK_1 radiation ($\lambda = 1.54056$ Å) was focused by a curved Ge(1 1 1) monochromator. For experiments using fast diffractometry a linear position sensitive detector (Stoe Mini PSD) was employed.

For dielectric studies capacitors were prepared from complexes **1**(12) and **1**(14) between two plane-parallel low resistance gold electrodes ($< 5\ \Omega$ sq.$^{-1}$) deposited on planar quartz glass plates with an area of $7 \times 13\,mm^2$ separated by 23 µm mica spacers. The capacity of the empty cell was strictly linear over the temperature range of our investigations. The cells were calibrated using toluene as reference (purified for spectroscopy) over the temperature range 20 to 50°C.

The capacitors were filled with samples that had been heated into the isotropic phase for one hour under vacuum to expel entrapped gases and residual solvents. Subsequent cooling gave recrystallized droplets that were then cut into stripes and transferred to the inlet of vertically mounted sample capacitors in a vacuum hot stage.

The sample capacitor was filled under vacuum at temperatures slightly above the clearing temperatures using gravity and capillary induced flow. The filling process was monitored by the HP 4192A self-balancing impedance analyser operating at 100 kHz and was generally complete within two hours. The complete filling of the cells was indicated from a saturation of the dielectric permittivity. Once filled, the cells were slowly cooled to room temperature under vacuum. The samples appeared to be stable under ambient atmosphere at temperatures below their clearing points. It was apparent that even under vacuum, long term exposures at high temperatures, i.e. days to weeks, resulted in degradation as indicated by the colour and texture changes.

The two mesogenic vanadyl complexes **1**(12) and **1**(14) were investigated using frequency domain dielectric spectroscopy (FDDS) from 10 mHz to 13 MHz. The computer controlled experimental apparatus consists of a HP4192A impedance analyser and a Schlumberger Solartron 1250 FRA in conjunction with a self-constructed amplifier based on the so-called Chelsea Dielectric Interface [25] principle. A Eurotherm 818 controller allowed temperature control for the dielectric measurements from room temperature to 200°C. The dielectric spectra were measured over the frequency range from 10 Hz to 10 MHz with 15 experimental points per decade. A total of 10 points per decade was used for the sub-Hertz experiments. Because vanadyl complexes change or decompose at high temperatures, the majority of the dielectric measurements were made under vacuum [26].

(*1*)

(*2*)

(*3*)

(*4*)

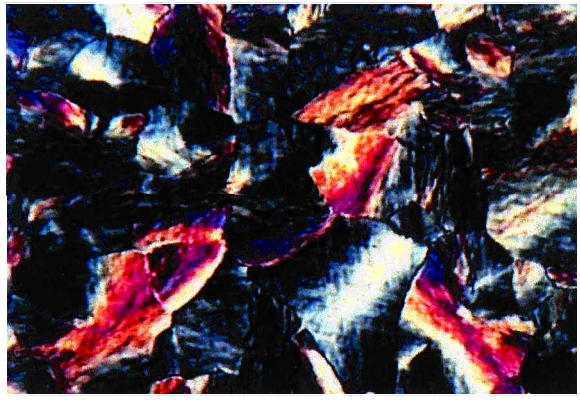

(*5*)

Figure 4. Colour plates. Photo 1—texture of the high temperature phase above the Col_{hd} phase of **1**(12) at 169.9°C; photo 2—texture of the less ordered Col_{rd} columnar phase of **1**(12) at 152.4°C; photo 3—texture of the col_{ro} columnar phase of **1**(12) at 147.1°C; photo 4—texture of the disordered crystalline Cr_x phase of **1**(12) at 100°C; photo 5—texture of the Cr_2 phase of **1**(12) at 60°C.

This allowed us to prevent oxidative degradation of the sample [27] giving the results with excellent reproducibility for all dielectric data.

The polarization reversal current measurements were performed while observing the samples with a polarizing microscope. The experimental conditions employed an optical hot stage, a controller, a function generator (Phillips PM 5188), and an oscilloscope HP 54603B with IEEE measurement storage module HP54666 and a computer. The parameters of the EHC cell used were

as follows: $A = 16\,\text{mm}^2$, $d = 10\,\mu\text{m}$ and $C_0 = 12.5$ pF. The voltage applied across the cell was $100\,V_{p\text{-}p}$. Systematic variation of the frequency and amplitude revealed the best experimental conditions. Exceeding 50 Hz, no process was visible. The resultant graphs were used for the calculation of the apparent spontaneous polarization with:

$$\mathbf{P}_s = \frac{\int I(t)\,dt}{2A} \tag{11}$$

where A is an effective area of the capacitor. The $\mathbf{P}_s$ is the integrated current per unit area after subtraction of the base line resistance and capacitance contributions [28].

4. Results and discussion

4.1. *X-ray diffraction investigations*

The structures of the compounds **1**(12) and **1**(14) were investigated by X-ray diffraction at several temperatures to characterize the mesophase types and structural parameters. The proposed indexing, the lattice constants, and the observed and calculated spacings are summarized in tables 2 and 3.

The compound **1**(12) exhibits three mesophases with the X-ray diffraction patterns shown in figure 5. The diffraction patterns of **1**(12) at 135 and 145°C showed many sharp reflections in the low angle region, attributed to a two dimensional rectangular lattice, and a diffuse halo at 4.6 Å. The mesophase at 135°C also exhibited a strong but broader reflection at 3.7 Å, which corresponds to the vanadyl–vanadyl repeating distance within the chain. The fact that this reflection is broader reflects a limited correlation length. Therefore, the mesophase at 135°C is identified as a discotic rectangular ordered columnar phase Col_{ro}. Upon entering the mesophase at 145°C the diffraction from the polymer repeating unit is lost, even though the V=O stretching mode indicates that the intermolecular correlation persists. The phase is characterized as a discotic rectangular disordered columnar mesophase Col_{rd}. The mesophase at 170°C showed three sharp peaks assignable to a two dimensional hexagonal lattice with lattice constant $a = 36.46$ Å. This mesophase also exhibited one broad peak at 4.6 Å, which corresponds to the molten alkyl chains. Therefore, this phase can be identified as a discotic hexagonal disordered columnar mesophase Col_{hd}. Again the short range structure was shown to persist in this phase by IR spectroscopy.

Two mesophases were found for **1**(14) and the X-ray diffraction patterns are shown in figure 6. The diffraction pattern at 110°C of **1**(14) showed several sharp reflections in the low angle region, a halo at 4.6 Å and a broad peak at 3.7 Å. Hence, we see a similar Col_{ro} mesophase to that found for **1**(12). Likewise the diffraction

Table 2. X-ray diffraction data of the complex **1**(12) (lattice constants, measured and calculated lattice spacings, and proposed indexing).

(*a*) Comparison of measured and calculated lattice spacings for the rectangular lattice of the mesophase at 135°C of **1**(12).

2θ/° (exp.)	2θ/° (calc.)	d/Å (exp.)	d/Å (calc.)	$h\,k\,l$
2.307	2.307	38.26	38.26	1 1 0
2.925	2.925	30.17	30.17	2 0 0
3.380	3.856	22.20	22.89	1 2 0
6.250	6.120	14.14	14.42	4 1 0
6.970	6.925	12.68	12.75	3 3 0
7.390	7.533	11.95	11.72	5 1 0
8.770	8.785	10.07	10.06	6 0 0
9.310	9.238	9.49	9.56	4 4 0
10.460	10.408	8.45	8.49	7 1 0
10.790	10.819	8.20	8.25	0 6 0
13.130	13.265	6.74	6.67	3 7 0
19.3		4.6 (broad)		
23.960	23.960	3.71	3.71	0 0 1

Col_{ro}: $a = 60.34$ Å, $b = 49.48$ Å, $c = 3.71$ Å

(*b*) Comparison of measured and calculated lattice spacings for the rectangular lattice of the mesophase at 145°C of **1**(12).

2θ/° (exp.)	2θ/° (calc.)	d/Å (exp.)	d/Å (calc.)	$h\,k\,l$
2.329	2.329	37.89	37.89	1 1 0
2.768	2.768	31.89	31.89	2 0 0
4.140	4.152	21.31	21.26	3 0 0
4.680	4.660	18.87	18.95	2 2 0
6.350	6.688	13.91	13.20	4 2 0
6.940	6.992	12.72	12.63	3 3 0
7.420	7.499	11.91	11.79	0 4 0
8.310	8.311	10.63	10.63	6 0 0
8.790	8.923	10.05	9.90	5 3 0
9.44	9.480	9.356	9.321	1 5 0
19.3		4.6 (broad)		

Col_{rd}: $a = 63.78$ Å, $b = 47.11$ Å

(*c*) Comparison of measured and calculated lattice spacings for the hexagonal lattice of the mesophase at 170°C of **1**(12).

2θ/° (exp.)	2θ/° (calc.)	d/Å (exp.)	d/Å (calc.)	$h\,k\,l$
2.796	2.795	31.58	31.58	1 0 0
4.850	4.840	18.21	18.23	1 1 0
7.500	7.401	11.78	11.93	2 1 0
19.3		4.6 (broad)		

Col_{hd}: $a = 36.46$ Å

Table 3. X-ray diffraction data of the complex **1**(14) (lattice constants, measured and calculated lattice spacings, and proposed indexing).

(*a*) Comparison of measured and calculated lattice spacings for the rectangular lattice of the mesophase at 110°C of **1**(14).

2θ/° (exp.)	2θ/° (calc.)	d/Å (exp.)	d/Å (calc.)	$h\,k\,l$
2.194	2.194	40.229	40.299	1 1 0
2.760	2.761	31.97	31.97	2 0 0
3.780	3.680	23.38	23.98	1 2 0
5.860	5.816	15.08	15.18	2 3 0
6.560	6.586	13.46	13.41	3 3 0
6.910	6.826	12.78	12.93	0 4 0
8.250	8.290	10.71	10.66	6 0 0
8.770	8.785	10.07	10.06	4 4 0
9.300	9.311	9.50	9.49	3 5 0
9.830	9.824	8.99	9.00	7 1 0
10.080	10.246	8.77	8.62	0 6 0
10.650	10.614	8.30	8.33	2 6 0
19.3		4.6 (broad)		
23.96	23.96	3.71	3.71	0 0 1

Col_{ro}: $a = 63.94$ Å, $b = 51.75$ Å, $c = 3.71$ Å

(*b*) Comparison of measured and calculated lattice spacings for the hexagonal lattice of the mesophase at 170°C of **1**(14).

2θ/° (exp.)	2θ/° (calc.)	d/Å (exp.)	d/Å (calc.)	$h\,k\,l$
2.741	2.741	32.20	32.20	1 0 0
4.750	4.749	18.58	18.59	1 1 0
19.3		4.6 (broad)		

Col_{hd}: $a = 37.18$ Å

at 170°C indicated a Col_{hd} phase with a lattice constant $a = 37.18$ Å and a halo at 4.6 Å. Again, although there were no clearly detectable diffractions due to the periodic long range order of the vanadyl chain, IR modes show some sort of intermolecular coupling.

4.2. *Phase transition evidence by conductivity measurements*

The phase transitions of both compounds also manifest changes in the low frequency conductivity σ measurements (figure 7) that correlated with the DSC measurements (figure 3). From room temperature to 100°C, the conductivities of all samples were in the range 10^{-9} to 10^{-10} S, indicating good insulator behaviour. The temperature dependence of σ for **1**(12) is illustrative (figure 7, top). In the Cr_x phase, the conductivity increases slightly with temperature. Upon further heating

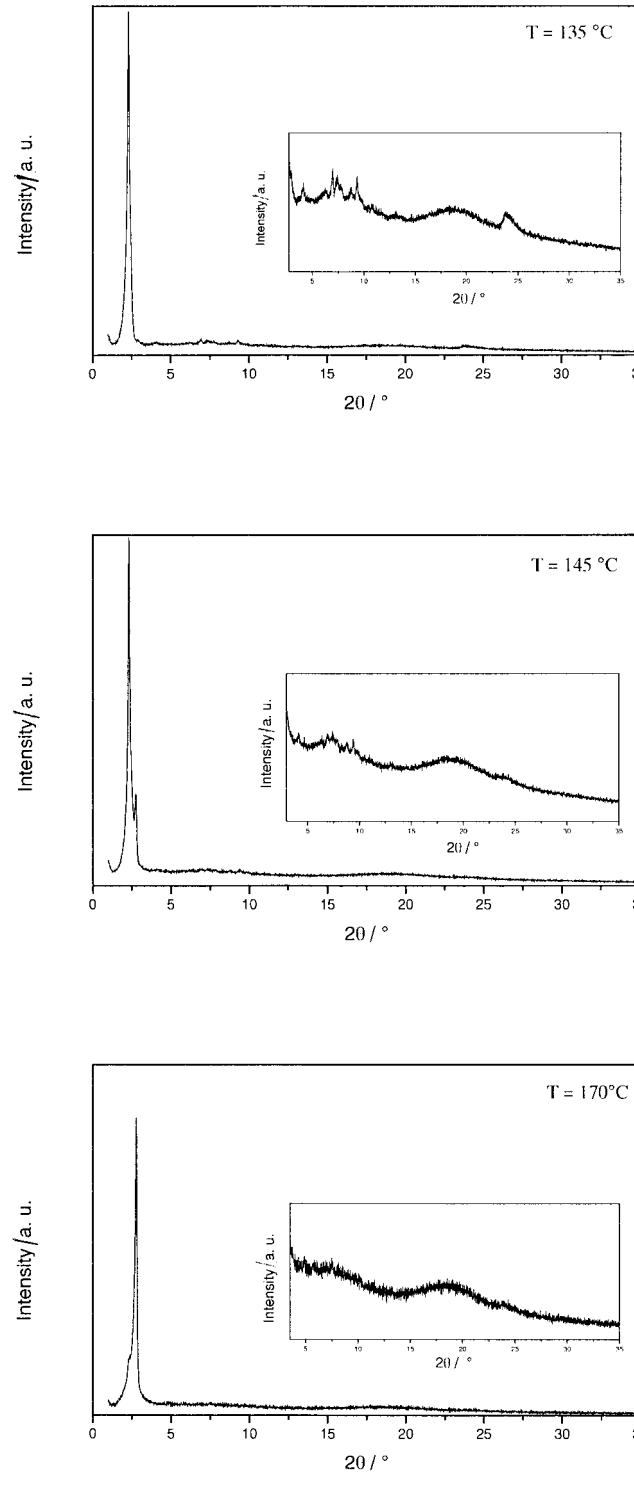

Figure 5. X-ray diffraction patterns of **1**(12) at selected temperatures 135, 145 and 170°C.

close to 100°C an inflection in the data for σ indicates a transition between the solid phase and the liquid crystalline Col_{ro} phase. The conductivity increases with

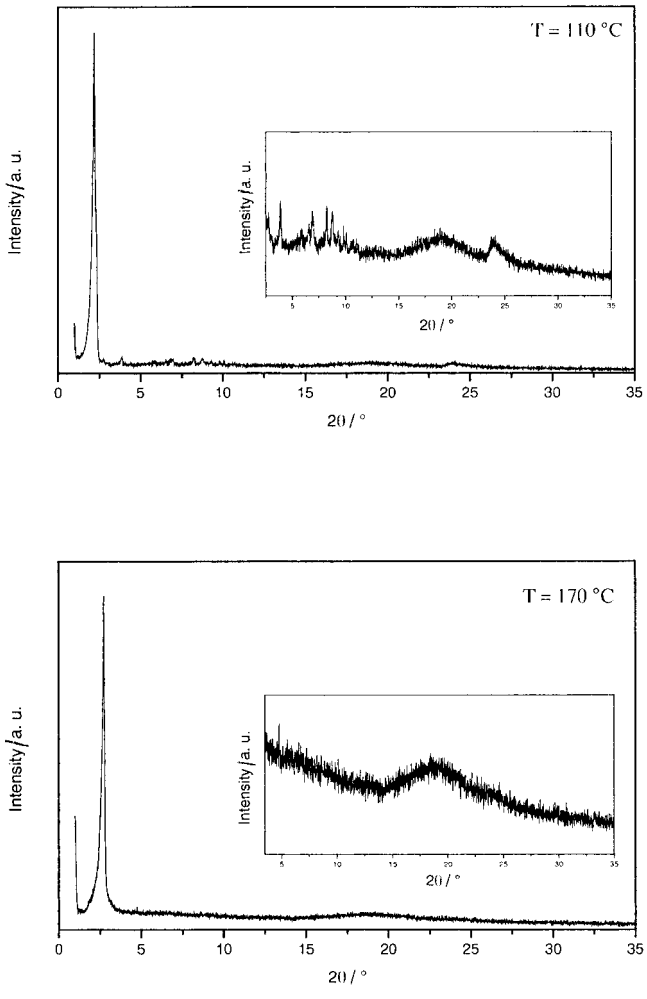

Figure 6. X-ray diffraction patterns of **1**(14) at selected temperatures 110 and 170°C.

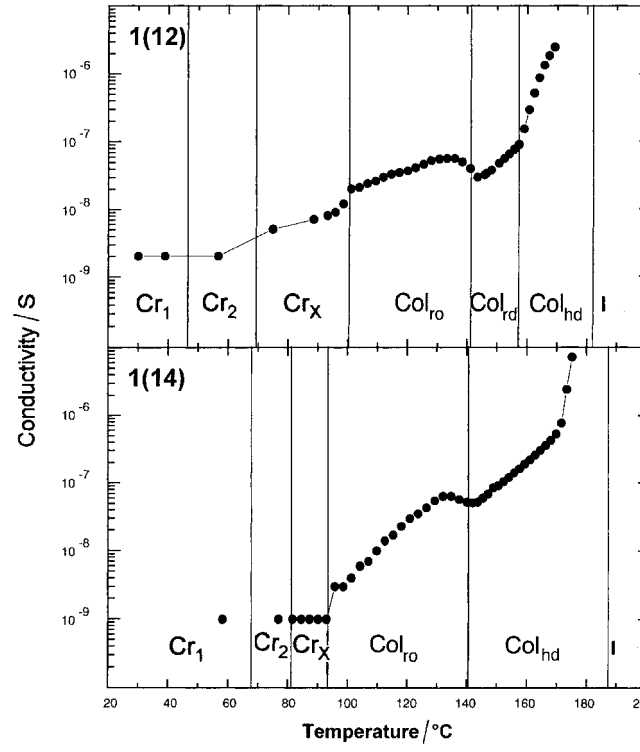

Figure 7. Temperature dependence of the electrical conductivity measured for **1**(12) and **1**(14) at low frequencies (20 Hz).

increasing temperature from 5×10^{-9} S in the Col_{ro} phase to 3×10^{-6} S in the Col_{rd} and Col_{hd} mesophases. The average activation energy was determined to be $E_1 = (93 \pm 3)$ kJ mol^{-1} for the Col_{ro} phase and $E_2 = (109 \pm 5)$ kJ mol^{-1} for the Col_{rd} phase, and this feature may be due to some breaking of the vanadyl chains. Recall that the XRD studies showed a loss of the strong vanadyl–vanadyl correlation. Therefore the contribution of the chain movement to conductivity is decreased. In the higher temperature Col_{hd} phase, there is a dramatic increase in conductivity which is probably due to decomposition on heating to a liquid-like phase, and this was also observed optically.

4.3. *Dielectric characterization*

From XRD it is known that the rectangular phases, Col_{ro} and Col_{rd}, respectively display a more ordered and a less ordered linear chain structure $(\text{---V=O---})_n$. Both phases are liquid crystalline, therefore the differences in dielectric properties reflect the mobility of the dipolar structure. In figure 8 (*a–c*) the dielectric relaxation processes of **1**(12) are shown as 3D plots for tan δ, ε' and ε'' versus frequency and temperature. According to equation (10) the transformation between (ε', tan δ) and (ε', ε'') shows that the absorption peaks for tan δ show up at higher frequencies, figure 8 (*a*), in comparison with the $\varepsilon''(\omega)$ spectrum, figure 8 (*b*). The dielectric modes observed for all mesophases of **1**(12) are annotated and are shown in a two-dimensional representation in figure 9. The processes denoted as **A**, **B**, **C** and **D** are related to liquid crystalline phases and the process **M** is related to the disordered crystalline phase Cr_x.

The crystalline phases at lower temperatures have a small conductivity and show no molecular reorientation. Intermediate between the crystal and liquid crystalline phases is an orientationally disordered crystalline (ODIC) phase Cr_x. This disordered phase arises because of molten alkoxy chains and is observed for both compounds. Its dielectric behaviour results from intramolecular reorientation of the alkoxy side chains in a similar way to the β-process of polymers. The change of the dielectric

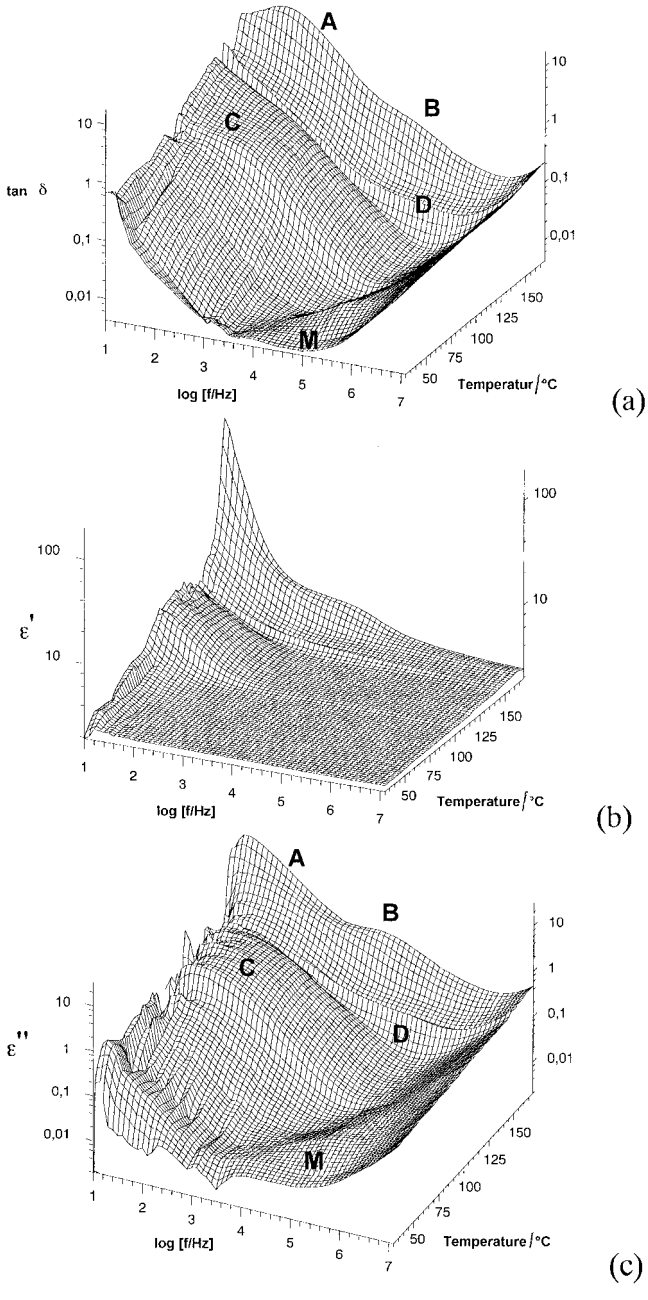

Figure 8. 3D plots of the dielectric spectra obtained for **1**(12). (*a*) Dielectric loss factor, (*b*) dispersion and (*c*) absorption.

permittivities at the Cr_x–Col_{ro} phase transition is due to a low frequency process (process **C**, figures 8 and 9) which is present only in the Col_{ro} phase.

The Col_{ro} phase can be characterized due to the low frequency process **C** (*vide infra*). This process is assigned as a 180° reorientation of the columnar polar chain. Reorientation about the molecular short axis appears to be frozen out in this phase. This phase can be supercooled to room temperature.

In the Col_{rd} phase of **1**(12), two pronounced dielectric relaxation processes **A** and **D** exist. **D** is a weak broad absorption process in the MHz range, see figures 8 (*a*–*c*). Due to its behaviour, this process is assigned as a rotational relaxation of the molecules inside the columns. Most probably this process is suppressed by the steric interactions of the longer alkyl chains of **1**(14) which does not exhibit such a phase. Process **A** is shifted to low frequencies and was checked by low frequency dielectric spectroscopy. Therefore it is absent in figures 8 (*a*–*c*).

For the Col_{hd}, phase of both substances, two lower frequency absorption peaks, i.e. processes **A** and **B**, are present. In the log–log 3D-plots of the dielectric spectra, figures 8 (*a*–*c*), a large dielectric absorption centred around 20 Hz (process **A**) is accompanied by a higher frequency absorption shoulder (process **B**). Both processes are strongly coupled and it is difficult to isolate them as separate contributions using a fitting program based on equation (8). However, it is possible to obtain reliable estimates for the relaxation times, taking into account that both relaxation processes have broad spectra and a distribution of relaxation times.

It is only possible to isolate the **B** process for **1**(12) at the highest temperature measurements due to the complex nature of the spectrum. This process, present at higher frequencies (> 10 kHz), is assigned to molecular reorientation of the molecules around their short axes and the activation of this process introduces the disorder in the polar chains in the columns. Therefore the long range polar order is broken in the lower viscosity Col_{hd} phases which have higher molecular and ionic mobility.

The dielectric spectra of **1**(12) in the sub-hertz frequency range shows a broad absorption peak **A** centred around 10^{-1} Hz. This absorption spans the wide frequency range from 10 Hz (figure 8 (*c*)) to 10 mHz (figure 10). We have not merged both spectra in one figure because they were acquired by using two different experimental systems (see § 3). The more fluid nature of the high temperature Col_{hd} mesophase enhances process **A**, which is connected with the relaxation of disrupted polar chains in the columns and also contains conductivity contributions. In addition, the large absorption at low frequencies indicates that this process is associated with interfacial polarization similar to the dielectric spectrum observed previously for liquid crystalline copper(II) Schiff's base complexes [13].

The temperature dependence of the static dielectric permittivity (figure 11, computed by fitting equation (9) to the dielectric spectra shown in figures 8 (*a*–*c*)) reveals dipole–dipole correlation between the columns. This effect was qualitatively described by the Fröhlich equation (6) adapted for one dimensional solids as explained earlier. The strong decrease of ε' on cooling from I to the Col_{hd}

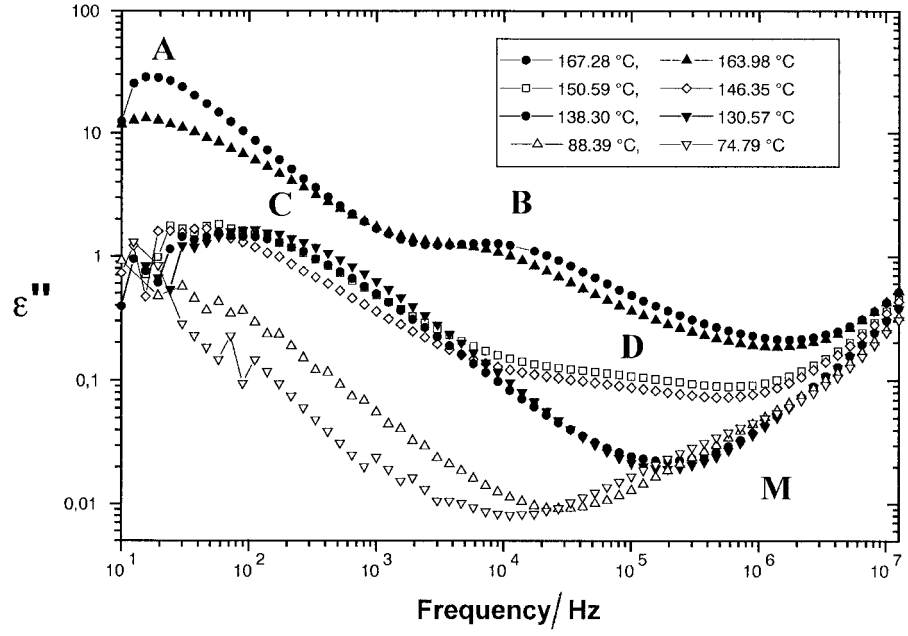

Figure 9. Overview of all Col phases and the Cr_x phase of **1**(12) with dielectric processes represented as absorption spectra at the temperatures given within the figure. Process **A**—defective chains + interfacial ionic polarization + conductivity (Col_{hd}); process **B**—molecular relaxation, reorientation about the short axes (Col_{hd}); process **C**—columnar relaxation (Col_{ro}); process **D**—molecular relaxation, rotation about the centre axes (Col_{rd}); process **M**—chain relaxation (the β-process) merged with a high frequency molecular process (Col_{rd}).

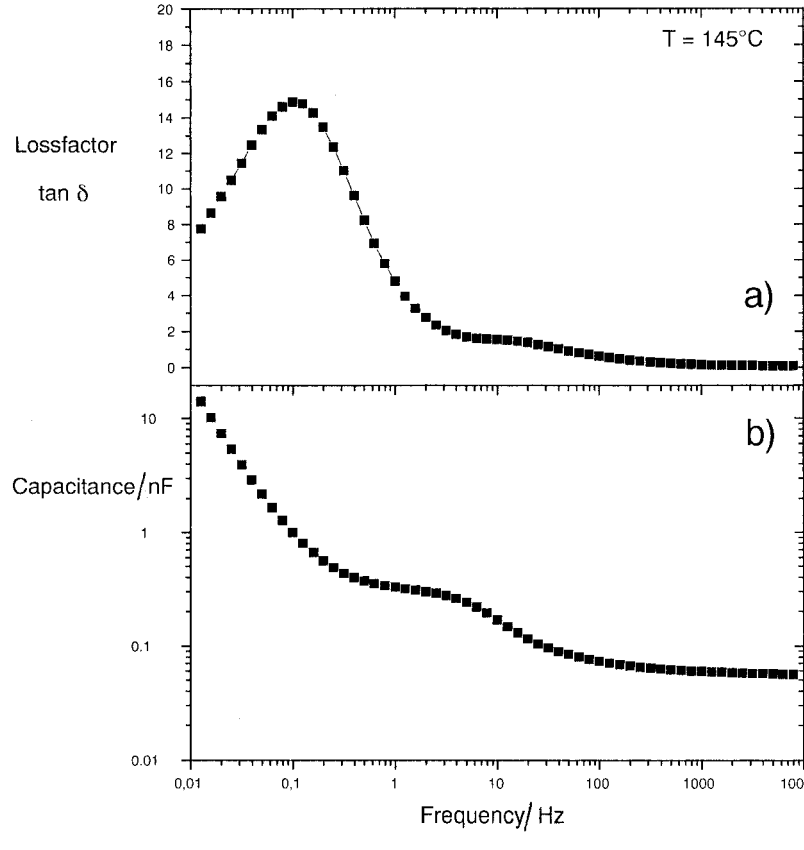

Figure 10. (*a*) Dielectric loss factor (upper curve) and (*b*) capacity (bottom curve) obtained in the sub-hertz frequency range for Col_{ro} phase of **1**(12).

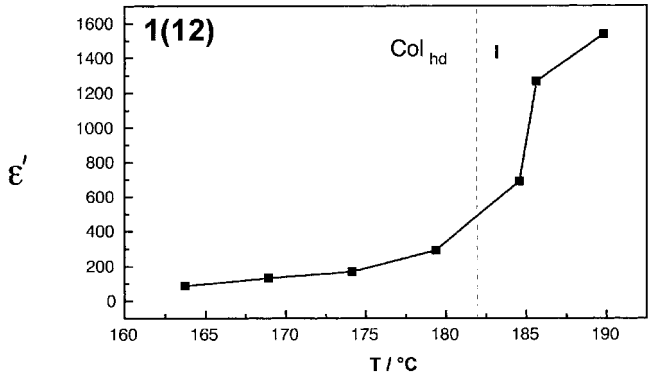

Figure 11. Temperature dependence of the static dielectric permittivity for the Col_{hd} and I phases of **1**(12).

phase (and from Col_{rd} to the Col_{ro} phase, not seen in figure 13) is connected with the antiparallel ordering of the columnar polarization vectors.

4.4. *Reversal current and switching experiments*

The low temperature Col_{ro} columnar phase shows characteristics of a ferroelectric phase and polarization switching induced by an applied voltage with a triangular waveform produces reversal current peaks, figure 12(*a*) [29]. The apparent spontaneous polarization calculated by integration of the current peaks is equal at most to *c.* 80 nC cm^{-2} for **1**(12) (see figure 13). An apparent polarization hysteresis plot, figure 12(*b*), is produced by integration of the reversal current. As seen in figure 13, the apparent spontaneous polarization decreases with decreasing temperature which could mean that in the Col_{ro} phase there is a negative dipole–dipole correlation ($g < 1$, equations (5) and (7)). The same behaviour was seen in the temperature dependence of the static dielectric constant (figure 11).

On the other hand, observation using the optical microscope indicated no movement in the optical texture by switching experiments. Moreover, reversal current experiments, like figure 12a, could only be fulfilled at low frequencies. In addition, behaviour as in figure 13 is slightly atypical. Therefore, another explanation involves ions/charges, simulating properties, as in figures 12 and 13.

All of our investigations support the conclusion that within the Col_{ro} phase there are one dimensional polar chains. The transition from Col_{ro} to the higher temperature phases results in a less-ordered rectangular lattice in the case of **1**(12) or a disordered hexagonal lattice in the case of **1**(14) which does not show any spontaneous polarization. In the Col_{rd} and Col_{hd} phases the long

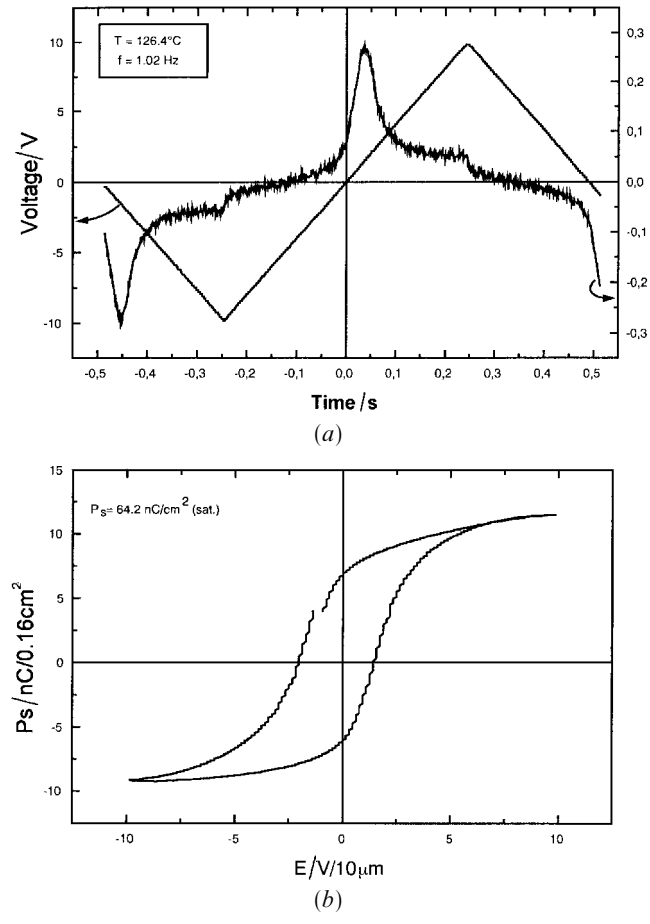

Figure 12. (*a*) Reversal current peaks observed for the Col_{ro} phase of **1**(12). (*b*) Computed hysteresis of polarization behaviour of **1**(12) at 126.4°C by taking into account the cell parameters (resistance and capacitance) and the reversal current spectrum.

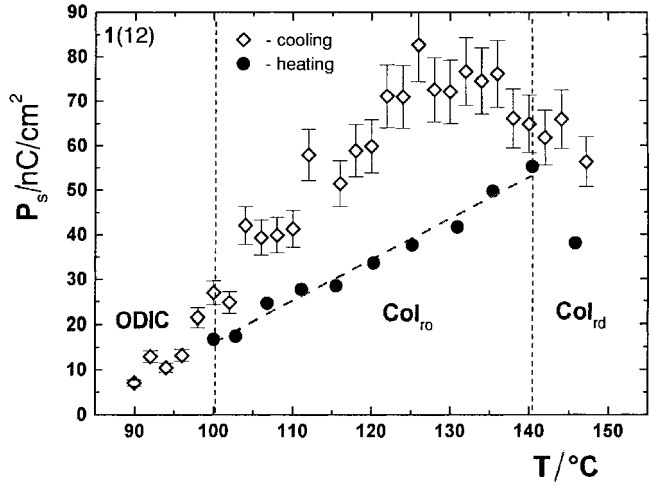

Figure 13. Temperature dependences of the apparent spontaneous polarization obtained on heating and cooling for **1**(12) by reversal current method.

range order of the chains is broken and this allows the reorientation of the molecule around its short axis and other rotational motions.

5. Summary

The studies reported herein establish the identity and dielectric response of three discotic columnar liquid crystalline phases, Col_{ro}, Col_{rd}, and Col_{hd} and a disordered crystalline phase Cr_x with dielectric response.

In general, compounds **1**(12) and **1**(14) display a complex dielectric spectrum. A summary of the dielectric relaxation studies is now given:

The crystalline phases of all the compounds investigated show very small conductivity and no molecular reorientation processes.

The Cr_x phases are orientationally disordered crystalline (ODIC) phases that display some intramolecular reorientation of terminal alkoxy chains which have local degrees of freedom shown in the X-ray investigations by broadening of the high angle reflections at 4.67 Å. These relaxations result in process **M** observed by dielectric spectroscopy. The change of the dielectric permittivities at the Cr_x–Col_{ro} phase transition are due to a low frequency collective process (process **C**, figure 9).

The Col_{ro} phase has been characterized by dielectric spectroscopy. The low frequency dielectric process **C** is typical and attributed to a 180° reorientation of the polar chains. Reorientation around the molecular short axis appears to be frozen out in this phase.

The Col_{rd} phase is observed only for **1**(12) and shows a weak dielectric absorption process **D** assigned to a rotational relaxation of the molecules inside the columns. At higher temperatures, the molecules relax more freely (see below) and in lower temperature phases, which are denser, these rotational motions are strongly hindered.

For the Col_{hd} phases the long range polar order is broken. The highly activated reorientation **B** around the molecular short axis is only observed in this more fluid phase and also enhances the low frequency conductive and interfacial polarization processes **A**.

In a further paper [29], we will present detailed results on a homologeous compound and we will return to the question of whether the reversal current experiments can be explained by ions/charges mobilities alone.

One of us (S.W.) would like to thank the DLR Buero in Bonn and KBN in Warsaw for financial support during his visit to Darmstadt University of Technology under the German–Polish Agreement (Pol-N-85-94). W.H., M.A.A. and D.K. would like to acknowledge the Deutsche Forschungsgemeinschaft (Ha-75-39b) for financial support. T.M.S. gratefully acknowledges support from the National Science Foundation and the Office of Naval Research.

References

[1] Meyer, R. B., Liebert, L., Strzelecki, L., and Keller, P., 1975, *J. Phys. (Paris)*, **36,** L69.
[2] Fukuda, A., Takanishi, Y., Isozaki, T., Ishikawa, K., and Takezoe, H., 1994, *J. mater. Chem.*, **4,** 997.
[3] Niori, T., Sekine, T., Watanabe, J., Furukawa, T., and Takezoe, H., 1996, *J. mater. Chem.*, **6,** 1231.
[4] Tournilhac, F., Blinov, L. M., Simon, J., and Yablonskii, S. V., 1992, *Nature*, **359,** 621.
[5] Soto Bustamante, E. A., Yablonskii, S. V., Ostrovski, B. I., Beresnev, L. A., Blinov, L. M., and Haase, W., 1996, *Chem. Phys. Lett.*, **260,** 447.
[6] Soto Bustamante, E. A., Yablonskii, S. V., Ostrovski, B. I., Beresnev, L. A., Blinov, L. M., and Haase, W., 1996, *Liq. Cryst.*, **21,** 829.
[7] Athanassopoulou, M. A., Hiller, S., Beresnev, L. A., Galyametdinov, Y. G., Schweißguth, M., and Haase, W., 1995, *Mol. Cryst. liq. Cryst.*, **261,** 29.
[8] Barbera, J., Iglesias, R., Serrano, J. L., Sierra, T., de la Fuente, M. R., Palacios, B., Perez Jubindo, M. A., and Vazquez, J. T., 1998, *J. Am. chem. Soc.*, **120,** 2908.
[9] Palacios, B., del la Fuente, M. R., Perez Jubindo, M. A., and Ros, M. B., 1997, *Liq. Cryst.*, **23,** 349; Palacios, B., de la Fuente, M. R., Perez Jubindo, M. A., Iglesias, R., Serrano, J. L., and Sierra, T., 1998, *Liq. Cryst.*, **25,** 481.
[10] Serette, A. G., Carroll, P. J., and Swager, T. M., 1992, *J. Am. chem. Soc.*, **114,** 1887.
[11] Zheng, H., Lai, C. K., and Swager, T. M., 1994, *Chem. Mater.*, **6,** 101.
[12] Serette, A. G., and Swager, T. M., 1993, *J. Am. chem. Soc.*, **115,** 8879.
[13] Borchers, B., 1991, PhD thesis, Technische Hochschule Darmstadt, Germany.
[14] Serette, A. G., 1994, PhD thesis, University of Pennsylvania, USA.
[15] Xu, B., and Swager, T. M., 1993, *J. Am. chem. Soc.*, **115,** 1159.
[16] Zheng, H., Caroll, P. J., and Swager, T. M., 1993, *Liq. Cryst.*, **14,** 1421.
[17] Serette, A. G., and Swager, T. M., 1994, *Angew. Chem., int. Ed. Engl.*, **33,** 2342.
[18] Knawby, D. A., 1996, PhD thesis, University of Pennsylvania, USA.
[19] Pfeiffer, M., Wròbel, S., Beresnev, A., and Haase, W., 1991, *Mol. Cryst. liq. Cryst.*, **202,** 193.
[20] Boettcher, C. J. F., and Bordewijk, P., 1978, *Theory of Electric Polarization*, Vol. I/II (Amsterdam-Oxford-New York: Elsevier).
[21] Fröhlich, H., 1958, *Theory of Dielectrics* (Oxford: Clarendon Press).
[22] Thoen, J., 1997, in *Handbook of Liquid Crystals*, Vol. 1, edited by D. Demus, J. W. Goodby, G. W. Gray, H.-W. Spiess and V. Vill (Weinheim: Wiley/VCH), Chap. VI.

[23] Klämke, W., Fan, Z. X., Haase, W., Müller, H. J., and Gallardo, H., 1989, *Ber. Bunsenges. Phys. Chem.*, **93,** 478.
[24] Fan, Z. X., and Haase, W., 1991, *J. chem. Phys.*, **95,** 6066.
[25] Pugh, J., 1979, *Automated digital dielectric measurements*, IEE-conference on dielectric materials, measurements and applications, Aston (England), 1979.
[26] Kilian, D., Wrobel, S., and Haase, W., (in preparation).
[27] West, A. R., 1992, *Grundlagen der Festkörperchemie* (Weinheim: VCH).
[28] Skarp, K., Dahl, I., Lagerwall, S. T., and Stebler, B., 1984, *Mol. Cryst. liq. Cryst.*, **114,** 283.
[29] Swager, T. M., Haase, W., Pozhidaer, E., and Wrobel, S. (to be published).